ISSN 1063-7834, Physics of the Solid State, 2014, Vol. 56, No. 10, pp. 2056–2063. © Pleiades Publishing, Ltd., 2014.
Original Russian Text © A.V. Malakhovskii, V.V. Sokolov, A.L. Sukhachev, A.S. Aleksandrovsky, I.A. Gudim, M.S. Molokeev, 2014, published in Fizika Tverdogo Tela, 2014, Vol. 56, No. 10, pp. 1991–1998.

OPTICAL PROPERTIES

Spectroscopic Properties and Structure of the $ErFe_3(BO_3)_4$ Single Crystal

A. V. Malakhovskii[a, *], V. V. Sokolov[b], A. L. Sukhachev[a], A. S. Aleksandrovsky[a], I. A. Gudim[a], and M. S. Molokeev[a]

[a] *Kirensky Institute of Physics, Siberian Branch of the Russian Academy of Sciences, Akademgorodok 50–38, Krasnoyarsk, 660036 Russia*

* *e-mail: malakha@iph.krasn.ru*

[b] *Siberian Federal University, pr. Svobodnyi 79, Krasnoyarsk, 660041 Russia*

Received April 16, 2014

Abstract—Single crystals of the $ErFe_3(BO_3)_4$ borate were synthesized and their structure was studied. Absorption spectra of the Er^{3+} ion in σ- and π-polarizations of *f–f* transitions $^4I_{15/2} \longrightarrow {}^4I_{13/2}$, $^4I_{11/2}$, $^4I_{9/2}$, $^4F_{9/2}$, $^4S_{3/2}$, $^2H_{11/2}$, and $^4F_{7/2}$ were measured. The refractive index and birefringence were measured as a function of the wavelength. The transition intensities were analyzed within the Judd–Ofelt theory, and the following parameters of the theory were obtained: $\Omega_2 = 7.056 \times 10^{-20}$ cm^2, $\Omega_4 = 1.886 \times 10^{-20}$ cm^2, and $\Omega_6 = 2.238 \times 10^{-20}$ cm^2. Using these parameters, the radiative transition probabilities, luminescence branching ratios, and radiative lifetimes of multiplets were calculated.

DOI: 10.1134/S1063783414100199

1. INTRODUCTION

Borates $RM_3(BO_3)_4$ (*R* is Y or rare-earth (RE) metal, and *M* is Al, Ga, Cr, Fe, or Sc) at high temperatures have a huntite structure with trigonal space group *R*32 (D_3^7) without inversion center. In some of them, structural phase transitions occur, reducing *R*32 symmetry to $R3_121$. The local symmetry of the RE ion environment has no inversion center as well. Therefore, parity-forbidden *f–f* transitions in RE ions of these crystals exhibit significant intensity and are widely used in optical quantum generators. Recently, we studied spectroscopic characteristics of the $ErAl_3(BO_3)_4$ crystal [1]. Since *f–f* transitions are allowed only due to the deviation of the local environment of the RE ion from the centrosymmetric one, the *f–f* transition intensities are very sensitive to crystal structure details. Therefore, it is of interest to clarify changes in the spectroscopic characteristics of the $ErAl_3(BO_3)_4$ crystal when substituting aluminum with iron. In addition to inevitable changes in the structural parameters, *d–d* transitions in the iron ion in the same spectral region and a strong absorption band caused by transitions with Fe–Fe charge transfer appear. The use of the Judd–Ofelt (J–O) theory makes it possible, having available only the spectra of *f–f* absorption from the ground state, to estimate the probabilities of the transitions between excited 4*f*-states.

The majority of ferroborates $RFe_3(BO_3)_4$ are multiferroics [2], i.e., they have simultaneously magnetic and electric polarizations. However, electric polarization in the $ErFe_3(BO_3)_4$ crystal is very small [2]. At the same time, the $ErAl_3(BO_3)_4$ crystal shows rather strong electric polarization in a magnetic field [3]. All RE ferroborates are magnetically ordered at temperatures below 30–40 K. In particular, $ErFe_3(BO_3)_4$ becomes an easy-plane antiferromagnet at temperature T_N = 38 K [4–6] (iron magnetic moments are in the plane perpendicular to the C_3 axis of the crystal). Magnetic properties of RE ferroborates have a significant effect on their optical properties, in particular, on the *f–f* transition spectra (see, e.g., [7–9]); the *f–f* transitions in the Er^{3+} impurity are widely used to study magnetic properties of different RE ferroborates (see, e.g., [4, 10]). However, to our knowledge, optical properties of the stoichiometric $ErFe_3(BO_3)_4$ crystal have not yet been studied.

2. EXPERIMENTAL TECHNIQUE, RESULTS, AND DISCUSSION

The $ErFe_3(BO_3)_4$ single crystals were grown by the solution–melt method using the technology described in [6].

The X-ray diffraction experiment was performed using a single-crystal diffractometer with a SMART APEXII two-coordinate detector operating with monochromatized MoK_α radiation, $\lambda = 0.7106$ Å. The opaque crystal had a prismatic habit 0.3 × 0.2 × 0.2 mm in size. The experiment was performed at room temperature.

Table 1. Main crystallographic characteristics and parameters of the experiment and refinement

Crystallographic parameters	
Chemical formula	$ErFe_3(BO_3)_4$
M_r	570.05
Space group, Z	$R32$, 3
a, Å	9.566(4)
c, Å	7.951(3)
V, Å^3	601.6(6)
D_x, Mg/cm^3	4.721
μ, mm	15.754
Sample size, mm	0.3 × 0.2 × 0.2
Data collection parameters	
Wavelength	MoK_α, λ = 0.7106 Å
Number of measured reflections	1911
Number of unique reflections	379
Number of reflections with $I > 2\sigma(I)$	379
Absorption correction	Multiscanning
R_{int}	0.0438
$2\theta_{max}$, deg	59.18
h	$-13 \longrightarrow 12$
k	$-13 \longrightarrow 13$
l	$-10 \longrightarrow 10$
Results of the refinement	
$R[F^2 > 2(F^2)]$	0.0166
$wR(F^2)$	0.0388
S	1.096
Weight	$w = 1/[\sigma^2(Fo^2) + (0.011P)^2 + 0.2P]$ where $P = (Fo^2 + 2Fc^2)/3$
Flack parameter [11]	0.11(2)
Number of refined parameters/restrictions	21/0
$(\Delta/\sigma)_{max}$	<0.001
$\Delta\rho_{max}$, e/Å^3	1.04
$\Delta\rho_{min}$, e/Å^3	−0.64
Extinction coefficient	0.0122(7)

D_x is the calculated sample density, μ is the X-ray absorption coefficient (MoK_α), R_{int} is the discrepancy factor according to intensities of equivalent reflections, $(\Delta/\sigma)_{max}$ is the maximum ratio of the displacement of the refined parameter to its standard deviation in the final refinement cycle, $\Delta\rho_{max}/\Delta\rho_{min}$ is the maximum/minimum difference electron density after the refinement of the structure.

The orientation matrix and unit cell parameters were determined and refined using 1672 reflections. The cell corresponded to the trigonal crystal system with rhombohedral centering. The main crystallographic characteristics, data collection parameters, and results of the refinement are given in Table 1.

The total experimental data were measured at an exposure of 10 s per frame. Each new frame was obtained by rotating the crystal about the ω axis by an angle of 0.5° at fixed angle φ. The range of variation in the angle of rotation about the ω axis was from 0 to 182°. A total of 364 frames were obtained for each of the angles φ = 0, 120°, and 240°. After that, the reflection intensity was integrated using the standard software of the device. Space group $R32$ was determined based on an analysis of extinctions and statistics of intensities of all reflections. The correction for X-ray absorption by the crystal was introduced from the analysis of intensities of equivalent reflections. After that, the intensities of equivalent reflections were averaged, and then only the unique reflections were used. Similar studies were previously performed for the $ErAl_3(BO_3)_4$ crystal [1].

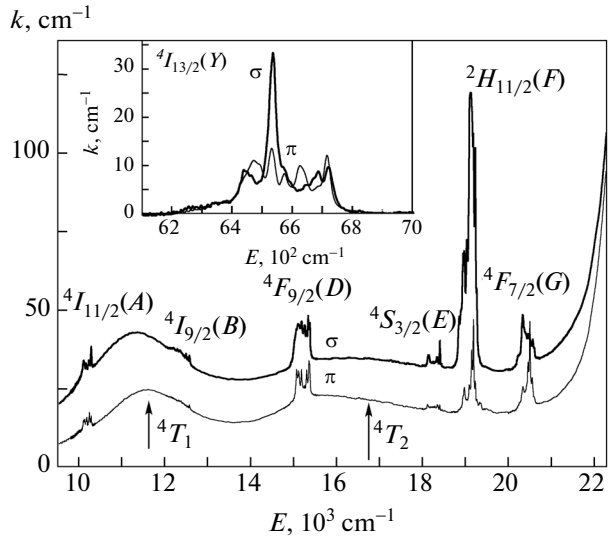

Fig. 1. Room-temperature polarized absorption spectra of the $ErFe_3(BO_3)_4$ crystal.

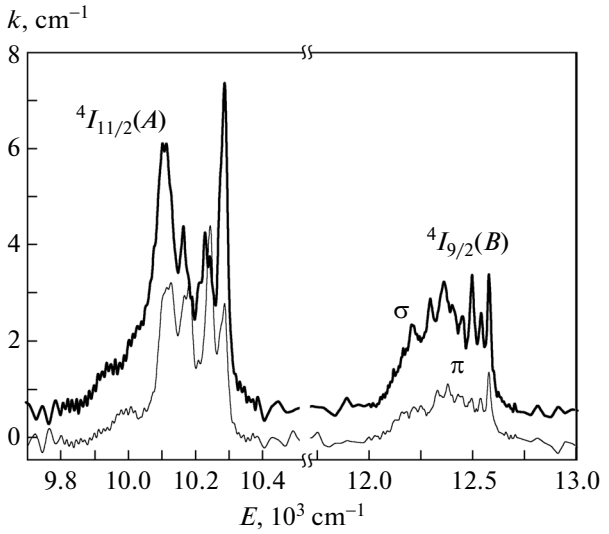

Fig. 2. Room-temperature polarized absorption spectra of f–f transitions $^4I_{15/2} \longrightarrow {}^4I_{11/2}, {}^4I_{9/2}$ in the Er^{3+} ion.

The model was sought using the SHELXS program [12] by direct methods. The structure obtained was refined by the least-squares method using the SHELXL97 program [12], taking into account the anisotropy of the thermal parameters of Er and Fe ions. Final factors of uncertainty and all main results are given in Table 1. The structure is deposited in the CSD databank with a number CSD-427565. The data can be obtained by the address: Fachinformationszentrum Karlsruhe, 76344 Eggenstein–Leopoldshafen, Germany (crystdata@fizkarlsruhe.de, http://www.fiz-karlsruhe.de/request_for_deposited_data.html).

The unit cell of the $ErFe_3(BO_3)_4$ crystal contains three formula units ($Z = 3$). Trivalent RE ions occupy only one site type with D_3 symmetry. RE ions are positioned at the center of the trigonal prism formed by six crystallographically equivalent oxygen ions. Each oxygen ion of the RE ion environment belongs to its borate group. The triangles formed by oxygen ions in neighboring basal planes are not overlapped with each other, but are rotated by a certain angle. Due to this distortion, D_{3h} symmetry of the ideal prism is reduced to D_3 [13].

For optical measurements, samples shaped as plane-parallel polished plates 0.2 mm thick oriented perpendicular and parallel to the third-order crystallographic axis were fabricated. The absorption spectra in the range of 9000–23000 cm^{-1} were measured using an automated two-beam spectrophotometer based on the MDR-2 monochromator. In the range of 6000–7000 cm^{-1}, the spectra were measured using a SHIMADZU UV-3600 spectrophotometer. The spectral resolution was ~10 cm^{-1}. The absorption spectra were measured under light propagating normally to the C_3 axis of the crystal for the light wave vector **E** parallel (π-spectrum) and perpendicular (σ-spectrum) to the C_3 axis and under light propagating along the C_3 axis (α-spectrum). The α- and σ-spectra coincide within experimental error, which points to the electric dipole absorption mechanism.

Figure 1 shows the absorption spectra (decimal absorption coefficient) of the crystal, measured at room temperature in the range from 6000 to 23000 cm^{-1}. The spectra consist of broad bands associated with the d–d transitions in iron ions ($^6A_1 \longrightarrow {}^4T_1$ and $^6A_1 \longrightarrow {}^4T_2$ in the notations of the cubic crystal field) and narrow f–f absorption bands. At $E \sim 22900$ cm^{-1}, the rather strong d–d transition $^6A_1 \longrightarrow {}^4A_1{}^4E$ occurs [14] (it was impossible to observe it at the sample thickness used in the present experiment). Then, (at $E \sim 25000$ cm^{-1}), strong absorption begins, caused by transitions with charge transfer between Fe^{3+} ions (Mott–Hubbard transitions) [14]. The bands of the d–d absorption were approximated by Gaussian curves and were subtracted from the total spectra. As a result, the f–f absorption band spectra shown in Figs. 2–4 were obtained. The absorption bands were identified based on the study by Kaminskii [15].

The intensities of the f–f absorption bands in π- and σ-polarizations were determined using the integrals $I = \int \frac{k(E)}{C} dE$ over bands, where C is the molar concentration of erbium ions (mol/L) and E is the light photon energy (cm^{-1}). The results are shown in Table 2. The transition intensities were averaged over polarizations according to the relation $I = (2I_\sigma + I_\pi)/3$ typical of uniaxial crystals. The oscillator strengths of

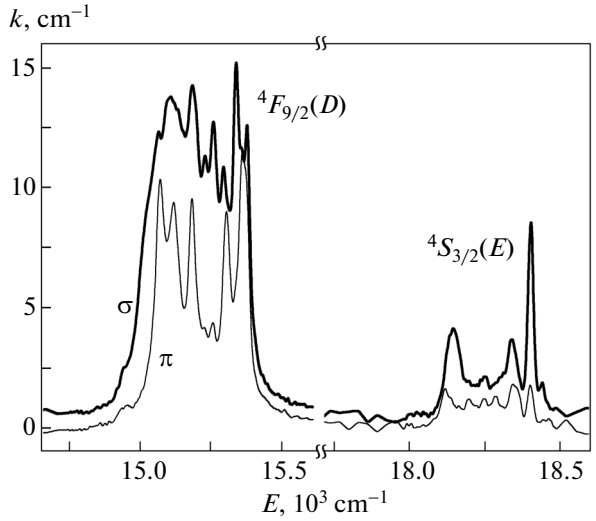

Fig. 3. Room-temperature polarized absorption spectra of f–f transitions $^4I_{15/2} \longrightarrow {}^4F_{9/2}, {}^4S_{3/2}$ in the Er^{3+} ion.

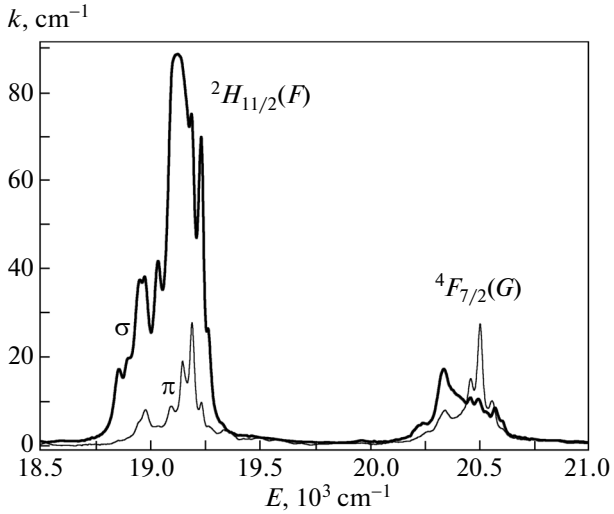

Fig. 4. Room-temperature polarized absorption spectra of f–f transitions $^4I_{15/2} \longrightarrow {}^2H_{11/2}, {}^4F_{7/2}$ in the Er^{3+} ion.

the $I \longrightarrow F$ transitions between J-multiplets were calculated by the formula [16]

$$f_{IF} = 4.318 \times 10^{-9} \frac{3n}{(n)^2 + 2} I_{IF}. \quad (1)$$

The refractive index n was determined by interference modulation of the flux passed through the sample (inset in Fig. 5). The condition of light amplification due to interference with the beam reflected from two boundaries has the form $2d = m\lambda/n$ or

$$m = 2nd/\lambda. \quad (2)$$

Here, d is the sample thickness, λ is the wavelength of light in vacuum, n is the crystal refractive index, and m is an integer. If the number m is large, $\Delta m = 2nd\Delta\lambda/\lambda^2$, where $\Delta\lambda$ is the distance between interference maxima, corresponding to the change in their number Δm. Then

$$n = \frac{\lambda^2 \Delta m}{2d\Delta\lambda}. \quad (3)$$

The measurement results are shown in Fig. 5. At wavelengths $\lambda < 700$ nm, the flux modulation becomes indistinguishable. The refractive index was determined at σ-polarization. The accuracy of this method is insufficient to reliably distinguish the refractive index at two polarizations. However, the birefringence Δn can be reliably determined by interference of ordinary and extraordinary beams. The sample cut out in parallel to the C_3 axis of the crystal, was placed between two polarizers with identical orientations of the polarization plane so that the latter would be at an

Table 2. Transition parameters: Γ_λ^2 are coefficients in the J–O equation (6), k_{IF} are the average wave numbers of absorption bands, I_{IF} are the total intensities of absorption bands, f_{IF} are the oscillator strengths of transitions, and s_{IF} are the transition strengths

Excited state	Γ_2^2	Γ_4^2	Γ_6^2	k_{IF}, cm^{-1}	I_{IF}, $cm^{-2}\,mol^{-1}\,L$		f_{IF}, 10^{-7}	s_{IF}, $10^{-20}\,cm^2$		
					π	σ		ErFeB (experiment)	ErFeB (calculation)	ErAlB (experiment [1])
$^4I_{13/2}(Y)$	0.0195	0.1173	1.4316	6570	358	417	17.16	3.85	3.563	4.57
$^4I_{11/2}(A)$	0.0282	0.0003	0.3953	10160	74	128	4.75	0.69	1.084	1.15
$^4I_{9/2}(B)$	0	0.1732	0.0099	12375	41	102	3.52	0.419	0.349	0.54
$^4F_{9/2}(D)$	0	0.5354	0.4619	15195	333	564	21.03	2.04	2.043	2.39
$^4S_{3/2}(E)$	0	0	0.2211	18290	46	87	3.16	0.255	0.495	0.374
$^2H_{11/2}(F)$	0.7125	0.4123	0.0925	19140	444	2491	78.11	6.02	6.012	5.65
$^4F_{7/2}(G)$	0	0.1468	0.6266	20430	424	438	18.71	1.35	1.679	1.62

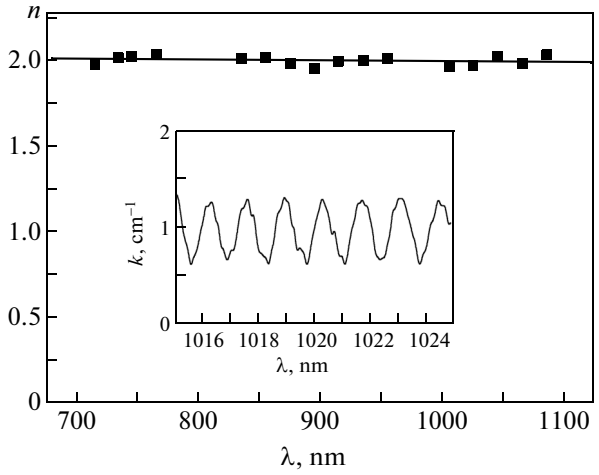

Fig. 5. Refractive index of $ErFe_3(BO_3)_4$. The inset shows interference modulation of the flux passed through the sample.

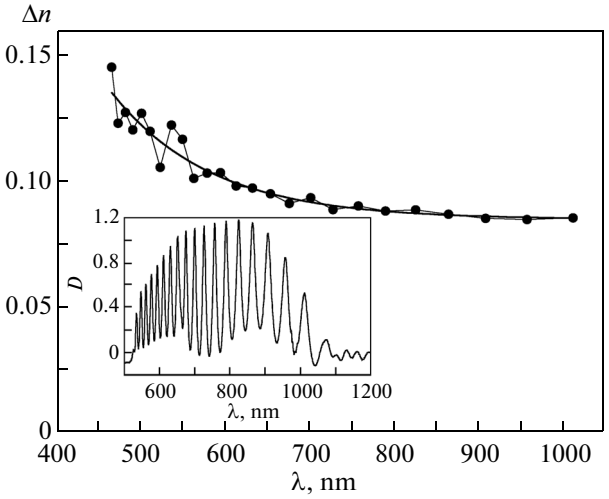

Fig. 6. Birefringence of the $ErFe_3(BO_3)_4$ crystal. The inset shows modulation of the flux passed through the sample due to interference of ordinary and extraordinary beams.

angle of 45° to the C_3 axis of the crystal. The result of interference of ordinary and extraordinary beams is shown in Fig. 6 (inset). The birefringence is determined from the distance between adjacent $\Delta\lambda$ maxima (or minima) by the formula [14]

$$\Delta n = \lambda^2/d\Delta\lambda. \quad (4)$$

The dependence of the birefringence on the wavelength, found in such a way, is shown in Fig. 6. Based on the data obtained, it can be considered that the refractive index is 2.0 with an error no more than ±0.13 in the whole studied spectral region. This yields an error of ±2% when determining oscillator strengths by formula (1). The oscillator strengths of transitions are presented in Table 2.

By definition, the transition strength is $s_{IF} = \frac{1}{e^2}\sum_{if}|\mathbf{D}_{if}|^2$, where $i \in I, f \in F$, and $\mathbf{D}_{ij}$ is the matrix element of the electric dipole moment. The transition strength and oscillator strength are related as [17]

$$s_{IF} = \frac{3hg_I}{8\pi^2 mck_{IF}} f_{IF}, \quad (5)$$

Table 3. Sum of strengths of seven transitions Σs, the Er–O distance between erbium ions and the nearest neighbor oxygen ions, and the angle α between bases of the triangular prism of oxygen ions, measured from the prism centrosymmetric state

Crystal	Σs, 10^{-20} cm^2	Er–O, Å	α, deg
$ErFe_3(BO_3)_4$	14.6	2.380(3)	47
$ErAl_3(BO_3)_4$	16.3	2.318(2)	44

where g_I is the degree of initial state degeneracy and k_{IF} is the average wavenumber of the absorption band. The experimentally determined *f–f* transition strengths are given in Table 2 along with transition strengths in $ErAl_3(BO_3)_4$. The largest difference is observed for *Y*, *B*, and *E* bands. Table 3 lists the sums of strengths of seven *f–f* transitions in $ErFe_3(BO_3)_4$ and $ErAl_3(BO_3)_4$ and the lattice parameters affecting the *f–f* transition intensity: the Er–O distance and the angle between the bases of the triangular prism of oxygen ions, measured from the centrosymmetric prism state. The largest value of this angle is 60°, i.e., the non-centrosymmetricity is close to maximum. We can see in Table 3 that the *f–f* transition intensity correlates with the Er–O distance (the shorter the distance, the higher the intensity).

Within the J–O theory, the *f–f* transition strength in the ion in the non-centrosymmetric crystal field is written as [18–20]

$$s_{IF} = \sum_{\lambda}\Omega_\lambda\Gamma_\lambda^2(I, F). \quad (6)$$

The coefficients $\Gamma_2^2(I, F) = \langle I|U^{(\lambda)}|F\rangle^2$ are calculated theoretically and are considered independent of the crystal structure. They are given in [15]. The subscript λ for *f–f* transitions takes three values: 2, 4, and 6. The considered transitions in the free Er^{3+} ion are not only parity-forbidden; most of them are forbidden by the total momentum due to the selection rules $\Delta J = 0, \pm 1$. However, according to the J–O theory, when transitions are parity-allowed due to the odd component of the crystal field, they can occur at $\Delta J \le \lambda$. In this approximation, all considered *f–f* transitions in the Er^{3+} ion are allowed. The transition $^4I_{15/2} \longrightarrow {}^2H_{11/2}$ is most intense (Fig. 1, Table 2). Indeed, it is a single

Table 4. J–O parameters of the Er^{3+} ion in different crystals

Crystal	Ω_2, 10^{-20} cm^2	Ω_4, 10^{-20} cm^2	Ω_6, 10^{-20} cm^2	References
$ErFe_3(BO_3)_4$	7.056	1.886	2.238	This work
$ErAl_3(BO_3)_4$	4.64	3.03	2.12	[1]
Er : $YAl_3(BO_3)_4$	8.38	1.61	1.50	[22]
Er : YAG	0.74	0.33	1.02	[23]
Er : YVO_4	13.45	2.33	1.67	[24]
Er : $YAlO_3$	0.95	0.58	0.55	[25]
Er : $LiNbO_3$	7.29	2.24	1.27	[26]

transition (among those considered in this paper) with a large coefficient Γ_2^2 (Table 2). Hence, the J–O parameter Ω_2 is relevant. This means that the first and third spherical harmonics t ($t = \lambda \pm 1$ [20]) in the crystal field expansion are involved in the parity allowing for the mentioned transition, whereas only higher harmonics are active in allowing other transitions.

From the set of Eqs. (6) written for all studied transitions, using the least-squares method [21], we determine the J–O parameters: $\Omega_2 = 7.056 \times 10^{-20}$ cm^2, $\Omega_4 = 1.886 \times 10^{-20}$ cm^2, and $\Omega_6 = 2.238 \times 10^{-20}$ cm^2 (see also Table 4 presenting the J–O parameters of some other crystals). Using these parameters and Eqs. (6), we solve the inverse problem, i.e., determine the theoretical values of transition strengths (Table 2). The root-mean-square error in the theoretical description of transition strengths is given by

$$\delta = \left[\frac{q\sum \Delta s^2}{(q-p)\sum s^2}\right]. \quad (7)$$

Here, q is the number of absorption bands, s are the measured transition strengths, Δs are the differences between measured and calculated transition strengths, and p is the number of determined parameters (three in the case at hand). Using Table 2, we find $\delta \approx 11\%$. It would seem that the error in the J–O description of the band intensity should decrease with increasing the number of measured absorption bands. However, in $ErAl_3(BO_3)_4$, where the intensities of 11 bands were measured, the error was 17% [1].

The equal populations of all components of the ground state splitting in the crystal field is one of the main postulates of the J–O theory; however, it is often unsatisfied in RE ions. In particular, the Er^{3+} ground state split in the $YAl_3(BO_3)_4$ crystal is 316 cm^{-1} (455 K) [27], i.e., this postulate is not satisfied even at room temperature. The second error source in the J–O description of the f–f transition intensity can be different temperature dependences of transition intensities. If the transition intensities vary with temperature in proportion to each other, it can be considered that the effective J–O parameters vary accordingly. The intensities of f–f transitions in $ErFe_3(BO_3)_4$ increase differently as the temperature increases from 90 to 270 K, i.e., from 1.1 to 1.6 (see Fig. 7), and do not reach a maximum at room temperature, which introduces an additional error to the J–O analysis. In $ErAl_3(BO_3)_4$, the absorption band intensities change even stronger [1].

Having known the parameters Ω_λ, using Eq. (6), we find the strengths of the transitions between excited states (Table 5). The parameters Γ_λ^2 were taken from [15]. The probability of the spontaneous dipole transition between degenerate levels in a condensed matter is given by the relation [28]

$$A_{IF} = \frac{64\pi^4 e^2 k_{IF}^3 n(k_{IF})}{3hg_I} s_{IF}. \quad (8)$$

Here, g_I is the initial multiplet degeneracy and $n(k_{IF})$ is the refractive index at the transition frequency. The values of k_{IF} for the transitions between excited levels were determined using the experimental obtained (Table 2).

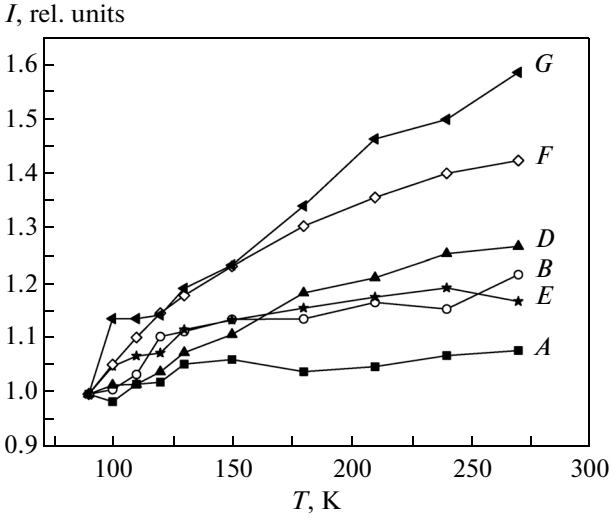

Fig. 7. Variation of the f–f transition intensities with increasing temperature.

Table 5. Transition wave numbers k_{IF} and strengths s_{IF}, spontaneous emission probabilities A, luminescence branching ratios β, and multiplet lifetimes τ

Initial level	Final level	k_{IF}, cm^{-1}	s_{IF}, 10^{-20} cm^2	A, s^{-1}	β, %	τ, ms
$^4I_{1/2}(Y)$	$^4I_{15/2}$	6570	3.563	91.38	100.00	10.94
$^4I_{11/2}$	$^4I_{13/2}$	3590	2.987	14.58	10.84	7.43
(*A*)	$^4I_{15/2}$	10160	1.084	119.99	89.16	
$^4I_{9/2}$	$^4I_{11/2}$	2215	0.433	0.59	0.48	8.03
(*B*)	$^4I_{13/2}$	5805	1.626	40.27	32.33	
	$^4I_{15/2}$	12375	0.349	83.70	67.20	
$^4F_{9/2}$	$^4I_{9/2}$	2820	0.976	2.77	0.28	0.992
(*D*)	$^4I_{11/2}$	5035	3.391	54.81	5.44	
	$^4I_{13/2}$	8625	0.520	42.26	4.19	
	$^4I_{15/2}$	15195	2.044	907.8	90.09	
$^4S_{3/2}$	$^4F_{9/2}$	3095	0.06	0.56	0.04	0.699
(*E*)	$^4I_{9/2}$	5915	0.717	47.01	3.29	
	$^4I_{11/2}$	8130	0.173	29.48	2.06	
	$^4I_{13/2}$	11720	0.774	394.84	27.61	
	$^4I_{15/2}$	18290	0.495	958.39	67.01	
$^2H_{11/2}$	$^4S_{3/2}$	850	0.397	0.02	≤0.1	0.214
(*F*)	$^4F_{9/2}$	3945	2.608	16.89	0.36	
	$^4I_{9/2}$	6765	2.23	72.85	1.56	
	$^4I_{11/2}$	8980	0.595	45.51	0.98	
	$^4I_{13/2}$	12570	0.395	82.88	1.78	
	$^4I_{15/2}$	19140	6.012	4448.13	95.32	
$^4F_{7/2}$	$^2H_{11/2}$	1290	0.863	0.29	0.01	0.358
(*G*)	$^4S_{3/2}$	2140	0.012	0.02	≤0.1	
	$^4F_{9/2}$	5235	0.184	4.17	0.15	
	$^4I_{9/2}$	8055	1.252	103.58	3.71	
	$^4I_{11/2}$	10270	0.863	147.99	5.30	
	$^4I_{13/2}$	13860	0.636	268.02	9.60	
	$^4I_{15/2}$	20430	1.679	2266.36	81.22	

The possibility of stimulated emission for an individual emission channel is characterized by the multiplet luminescence branching ratio

$$\beta_{IF} = A_{IF}\Big/\sum_F A_{IF} = A_{IF}\tau_I, \qquad (9)$$

where τ_I is the excited state lifetime. The calculated transition strengths, spontaneous emission probabilities, transition branching ratios, and lifetimes are given in Table 5. The largest branching ratios are inherent to ground-state transitions; however, there are transitions between excited states with significant (>10%) branching ratios: $^4I_{11/2} \longrightarrow {}^4I_{13/2}$; $^4I_{9/2} \longrightarrow {}^4I_{13/2}$; $^4S_{3/2} \longrightarrow {}^4I_{13/2}$. Luminescence was not experimentally detected, probably, due to luminescence quenching by *d*–*d* transitions in iron ions.

3. CONCLUSIONS

The $ErFe_3(BO_3)_4$ single crystals were synthesized and their structure was studied. The absorption spectra of the Er^{3+} ion in σ- and π-polarizations of *f*–*f* transitions $^4I_{15/2} \longrightarrow {}^4I_{13/2}$, $^4I_{11/2}$, $^4I_{9/2}$, $^4F_{9/2}$, $^4S_{3/2}$, $^2H_{11/2}$, and $^4F_{7/2}$ were measured. The refractive index and birefringence were measured by interference methods as functions of wavelength. It was found that there is a correlation between the intensity of *f*–*f* transitions and the Er–O distance in the isostructural crystals $ErFe_3(BO_3)_4$ and $ErAl_3(BO_3)_4$. The transition intensities were analyzed within the Judd–Ofelt theory, and the following parameters of the theory were obtained: $\Omega_2 = 7.056 \times 10^{-20}$ cm^2, $\Omega_4 = 1.886 \times 10^{-20}$ cm^2, and $\Omega_6 = 2.238 \times 10^{-20}$ cm^2. Using these parameters, the radiative transition probabilities, luminescence

branching ratios, and radiative lifetimes of multiplets were calculated. It was shown that the error in the J–O analysis of the *f–f* absorption spectra depends strongly on the difference between the temperature dependences of the *f–f* transition intensity.

ACKNOWLEDGMENTS

This study was supported by the Russian Foundation for Basic Research (project no. 12-02-00026), the Council on Grants from the President of the Russian Federation for Support of Leading Scientific Schools (grant no. NSh-2886.2014.2), and the Department of Physical Sciences of the Russian Academy of Sciences (program no. 3.9.5).

REFERENCES

1. A. V. Malakhovskii, T. V. Kutsak, A. L. Sukhachev, A. S. Aleksandrovsky, A. S. Krylov, I. A. Gudim, and M. S. Molokeev, Chem. Phys. **428**, 137 (2014).
2. A. M. Kadomtseva, Yu. F. Popov, G. P. Vorob'ev, A. P. Pyatakov, S. S. Krotov, K. I. Kamilov, V. Yu. Ivanov, A. A. Mukhin, A. K. Zvezdin, A. M. Kuz'menko, L. N. Bezmaternykh, I. A. Gudim, and V. L. Temerov, Low Temp. Phys. **36** (6), 511 (2010).
3. K.-C. Liang, R. P. Chaudhury, B. Lorenz, Y. Y. Sun, L. N. Bezmaternykh, I. A. Gudim, V. L. Temerov, and C. W. Chu, J. Phys: Conf. Ser. **400**, 032046 (2012).
4. M. N. Popova, E. P. Chukalina, T. N. Stanislavchuk, and L. N. Bezmaternykh, J. Magn. Magn. Mater. **300**, e440 (2006).
5. E. A. Popova, A. N. Vasiliev, V. L. Temerov, L. N. Bezmaternykh, N. Tristan, R. Klingeler, and B. Büchner, J. Phys.: Condens. Matter **22**, 116006 (2010).
6. C. Ritter, A. Vorotynov, A. Pankrats, G. Petrakovskii, V. Temerov, I. Gudim, and R. Szymczak, J. Phys.: Condens. Matter **22**, 206002 (2010).
7. M. N. Popova, E. P. Chukalina, T. N. Stanislavchuk, B. Z. Malkin, A. R. Zakirov, E. Antic-Fidancev, E. A. Popova, L. N. Bezmaternykh, and V. L. Temerov, Phys. Rev. B: Condens. Matter **75**, 224435 (2007).
8. A. V. Malakhovskii, S. L. Gnatchenko, I. S. Kachur, V. G. Piryatinskaya, A. L. Sukhachev, and V. L. Temerov, Eur. Phys. J. B **80**, 1 (2011).
9. A. V. Malakhovskii, S. L. Gnatchenko, I. S. Kachur, V. G. Piryatinskaya, A. L. Sukhachev, and I. A. Gudim, J. Alloys Compd. **542**, 157 (2012).
10. T. N. Stanislavchuk, E. P. Chukalina, M. N. Popova, L. N. Bezmaternykh, and I. A. Gudim, Phys. Lett. A **368**, 408 (2007).
11. H. D. Flack, Acta Crystallogr., Sect. A: Found. Crystallogr. **39**, 876 (1983).
12. G. M. Sheldrick, Acta Crystallogr., Sect. A: Found. Crystallogr. **64**, 112 (2008).
13. I. Couwenberg, K. Binnemans, H. De Leebeeck, and C. Görller-Walrand, J. Alloys Compd. **274**, 157 (1998).
14. A. V. Malakhovskii, A. L. Sukhachev, A. D. Vasil'ev, A. A. Leont'ev, A. V. Kartashev, V. L. Temerov, and I. A. Gudim, Eur. Phys. J. B **85**, 80 (2012).
15. A. A. Kaminskii, *Crystalline Lasers: Physical Processes and Operating Schemes* (CRC Press, New York, 1996).
16. A. V. Malakhovskii, A. E. Sokolov, V. L. Temerov, L. N. Bezmaternykh, A. L. Sukhachev, V. A. Seredkin, S. L. Gnatchenko, I. S. Kachur, and V. G. Piryatinskaya, Phys. Solid State **50** (7), 1287 (2008).
17. I. I. Sobelman, *Introduction to the Theory of Atomic Spectra* (Pergamon, London, 1972; Nauka, Moscow, 1977).
18. B. R. Judd, Phys. Rev. **127**, 750 (1962).
19. G. S. Ofelt, J. Chem. Phys. **37**, 511 (1962).
20. R. D. Peacock, Struct. Bonding (Berlin) **22**, 83 (1975).
21. W. F. Krupke, IEEE J. Quantum Electron. **QE-7**, 153 (1971).
22. W. You, Y. Lin, Y. Chen, Z. Luo, and Y. Huang, Opt. Mater. **29**, 488 (2007).
23. D. K. Sardar, W. M. Bradley, J. J. Perez, J. B. Gruber, B. Zandi, J. A. Hutchinson, C. W. Trussell, and M. R. Kokta, J. Appl. Phys. **93**, 2602 (2003).
24. J. A. Capobianco, P. Kabro, F. S. Ermeneux, R. Moncorge, M. Bettinelli, and E. Cavalli, Chem. Phys. **214**, 329 (1997).
25. A. A. Kaminskii, V. S. Mironov, A. Kornienko, S. N. Bagaev, G. Boulon, A. Brenier, and B. Di Bartolo, Phys. Status Solidi A **151**, 231 (1995).
26. J. Amin, B. Dussardier, T. Scweizer, and M. Hempstead, J. Lumin. **69**, 17 (1996).
27. A. Baraldi, R. Capelletti, N. Magnani, M. Mazzera, E. Beregi, and I. Földvári, J. Phys.: Condens. Matter **17**, 6245 (2005).
28. V. L. Ginzburg, *Theoretical Physics and Astrophysics* (Nauka, Moscow, 1975; Pergamon, London, 1979).

Translated by A. Kazantsev